

LATENT IMAGE ANIMATOR: LEARNING TO ANIMATE IMAGES VIA LATENT SPACE NAVIGATION

Anonymous authors

Paper under double-blind review

ABSTRACT

Due to the remarkable progress of Generative Adversarial Networks (GANs) and auto-encoder animating images has become increasingly efficient, whereas associated results have become increasingly realistic. Current animation-approaches commonly exploit structure representation extracted from driving videos. Such structure representation (*e.g.*, keypoints or regions) is instrumental in transferring motion from driving videos to still images. However, such approaches fail in case that a source image and driving video encompass large appearance variation. Moreover, the extraction of structure information requires additional modules that endow the animation-model with increased complexity. Deviating from such models, we here introduce the Latent Image Animator (LIA), a self-supervised auto-encoder that evades need for structure representation. LIA is streamlined to animate images by linear navigation in the latent space. Specifically, motion in generated video is constructed by linear displacement of codes in the latent space. Towards this, we learn a set of orthogonal motion directions simultaneously, and use their linear combination, in order to represent any displacement in the latent space. Extensive quantitative and qualitative analysis suggests that our model systematically and significantly outperforms state-of-art methods on VoxCeleb, Taichi and TED-talk datasets *w.r.t.* generated quality.

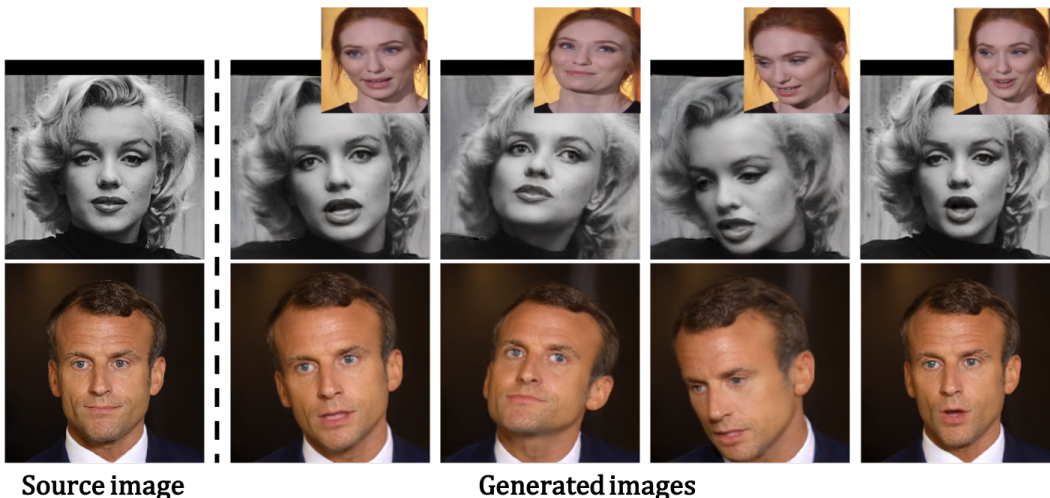


Figure 1: **LIA animation examples.** Two example images animated by LIA, which transfers motion of a driving video (smaller images on the top) from VoxCeleb dataset (Chung et al., 2018) onto still images of two celebrities, Marilyn Monroe and Emmanuel Macron. LIA is able to successfully animate these two images without relying on any *explicit structure representations*, such as landmarks and region representations

1 INTRODUCTION

In the series of science fiction books *Harry Potter* (Rowling et al., 2016; Rowling, 2019), wizards and witches were able to magically *enchant portraits, bringing them to life*. Remarkable progress of deep generative models has recently turned this vision into reality. This work examines the scenario where a framework animates a *source image* by motion representations learned from a *driving video*. Existing approaches for *image animation* are classically related to computer graphics (Cao et al., 2014; Thies et al., 2016; 2019) or exploit explicit *structure representations* such as labels (Wang et al., 2020a), semantic maps (Pan et al., 2019; Wang et al., 2018; 2019), human key-points (Jang et al., 2018; Yang et al., 2018; Walker et al., 2017; Chan et al., 2019; Zakharov et al., 2019; Wang et al., 2019; Siarohin et al., 2019), 3D face mesh (Zhao et al., 2018) and optical flow (Li et al., 2018; Ohnishi et al., 2018). We note that the ground truth of such structure representations is being computed a-priori for the purpose of supervised training. This poses constraints on applications, where such representations of unseen testing images might be fragmentary or missing.

Self-supervised motion transfer approaches (Wiles et al., 2018; Siarohin et al., 2019; 2021) accept raw videos as input and learn to reconstruct driving images by warping source image with predicted *dense flow fields*. While the need for domain knowledge or labeled ground truth data has been obviated (improving performance on in-the-wild testing images), such methods entail necessity of explicit structure representations as motion guidance. Prior information such as keypoints or regions are learned in an end-to-end training manner by additional networks as intermediate features, in order to predict target flow fields. Although online prediction of such representations is less tedious than the acquisition of ground truth labels, it still strains the complexity of networks.

Deviating from such approaches, we here aim to fully *eliminate* the need of *explicit structure representations* by directly manipulating the latent space of a deep generative model. To the best of our knowledge, this constitutes a new direction in the context of *image animation*. Our work is motivated by *interpretation of GANs* (Shen et al., 2020; Goetschalckx et al., 2019; Jahanian et al., 2020; Voynov & Babenko, 2020), showcasing that latent spaces of StyleGAN (Karras et al., 2019) and BigGAN (Brock et al., 2019) contain rich semantically meaningful directions. Given that walking along such directions, basic visual transformations such as *zooming* and *rotation* can be induced in generated results. As in image animation, we have that *motion* between source and driving images can be considered as higher-level transformation, a natural question here arises: can we discover a set of directions in the latent space of an image animator that induces high-level transformations collaboratively?

Towards answering this question, we introduce a novel Latent Image Animator (LIA), constituting of an auto-encoder for animating still images via latent space navigation. LIA seeks to animate a source image via linearly navigating associated source latent code along a learned latent path to reach a target latent code, which represents the high-level transformation for animating the source image. We introduce a Linear Motion Decomposition (LMD) approach aiming to represent a latent path via a linearly combination of a set of learned motion directions and associated magnitudes. Specifically, we constrain the set as an orthogonal basis, where each vector indicates a basic visual transformation. By describing the whole motion space using such learned basis, LIA eliminates the need of explicit structure representations.

In addition, we design LIA to *disentangle motion and appearance* within a single encoder-generator architecture. Deviating from existing methods using separate networks to learn disentangled features, LIA integrates both, latent *motion* code, as well as *appearance* features in a *single encoder*, which highly *reduces the model complexity* and simplifies training.

We provide evaluation on multiple datasets including VoxCeleb, TaichiHD and TED-talk. In addition, we show that LIA outperforms the state-of-the-art in preserving the facial structure in generated videos in the setting of one-shot image animation on unseen dataset (FFHQ and GermanAudio).

2 RELATED WORK

Video generation Generative adversarial networks (GAN)-based video generation is aimed at mapping Gaussian noise to video, directly and in the absence of prior information (Vondrick et al., 2016; Saito et al., 2017; Tulyakov et al., 2018; Wang et al., 2020b). Recently, with the progress of GANs in photo-realistic image generation (Brock et al., 2019; Karras et al., 2019; 2020), a series of works (Clark et al., 2019; Wang et al., 2021b) explored production of high-resolution videos by incorporating the architecture of an *image generator* into *video GANs*, trained jointly with RNNs. Tian et al. (2021) directly leveraged the knowledge of a pre-trained StyleGAN to produce videos of resolution up to 1024×1024 . Unlike these approaches, which generate random videos based on

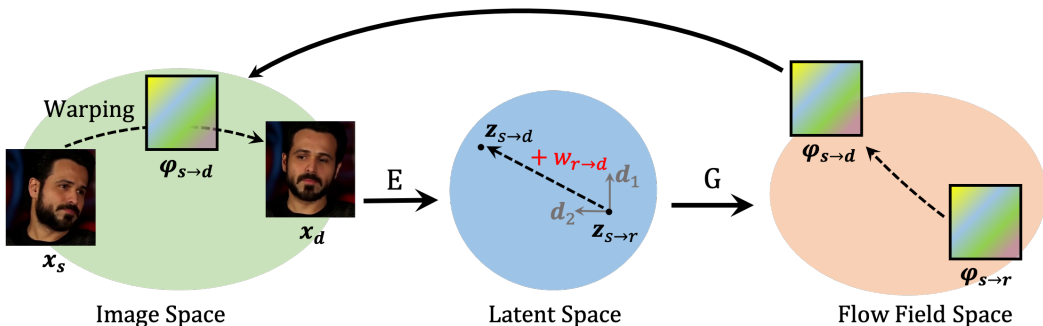


Figure 2: **General pipeline.** Our objective is to transfer motion via latent space navigation. The entire training pipeline consists of two steps. In the first step, we encode a source image x_s into a latent code $z_{s \rightarrow r}$. By linearly navigating $z_{s \rightarrow r}$ along a path $w_{r \rightarrow d}$, we reach a target latent code $z_{s \rightarrow d}$. The latent paths are represented by a linear combination between a set of learned motion directions, which is an orthogonal basis, and associated magnitudes. In the second step, we decode $z_{s \rightarrow d}$ to a target dense optical flow field $\phi_{s \rightarrow d}$, which is used to warp x_s into a driving image x_d . While we train our model using images from the same video sequence, in the testing phase x_s and x_d generally pertain to different identities.

noise vectors in an unconditional manner, in this paper, we focus on conditionally creating novel videos by transferring motion from driving videos to input images.

Latent space editing In an effort to control generated images, recent works explored the discovery of semantically meaningful directions in the latent space of pre-trained GANs, where linear navigation corresponds to desired image manipulation. Supervised (Shen et al., 2020; Jahanian et al., 2020; Goetschalckx et al., 2019) and unsupervised (Voynov & Babenko, 2020; Peebles et al., 2020; Shen & Zhou, 2021) approaches were proposed to edit semantics such as facial attributes, colors and basic visual transformations (*e.g.*, rotation and zooming) in generated or inverted real images (Zhu et al., 2020; Abdal et al., 2020). In this work, as opposed to finding directions corresponding to individual visual transformations, we seek to learn a set of directions that cooperatively allows for high-level visual transformations that can be beneficial in image animation.

Image animation Related approaches (Chan et al., 2019; Wang et al., 2018; Zakharov et al., 2019; Wang et al., 2019) in image animation required strong prior structure labels as motion guidance. In particular, Chan et al. (2019) and Wang et al. (2018) proposed to map representations such as human keypoints and facial landmarks to videos in the setting of image-to-image translation proposed by Isola et al. (2017). However, such approaches were only able to learn an individual model for a single identity. Transferring motion on new appearances requires retraining the entire model from scratch by using videos of target identities. Several recent works (Zakharov et al., 2019; Wang et al., 2019) explored meta learning in fine-tuning models on target identities. While only few images of target identities were required during inference time, it was still compulsory to input pre-computed structure representations in those approaches, which usually are hard to access in many real-world scenarios.

Towards addressing this issue, very recent works (Siarohin et al., 2019; 2021; Wang et al., 2021a; Wiles et al., 2018) proposed to learn image animation in self-supervised manner, only relying on RGB videos for both, training and testing without any priors. They firstly predicted dense flow fields from input images, which were then utilized to warp source images, in order to obtain final generated results. Inference only required one image of a target identity without any fine-tuning step on pre-trained models. While no priors were required, state-of-the-art methods still followed the idea of using explicit structure representations. FOMM (Siarohin et al., 2019) proposed a first order motion approach to predict keypoints and local transformations online to generate flow fields. Siarohin et al. (2021) developed this idea to model articulated objects by replacing a keypoints predictor by a PCA-based region prediction module. Wang et al. (2021a) extended FOMM by predicting 3D keypoints for view-free generation. We note though that in all approaches, given that keypoints or regions are inadequately predicted, the quality of generated images drastically decreases. In contrast to such approaches, our method does not require any explicit structure representations. We dive into the latent space of the generator and self-learn to navigate motion codes in certain directions with the goal to reach target codes, which are then decoded to flow fields for warping.

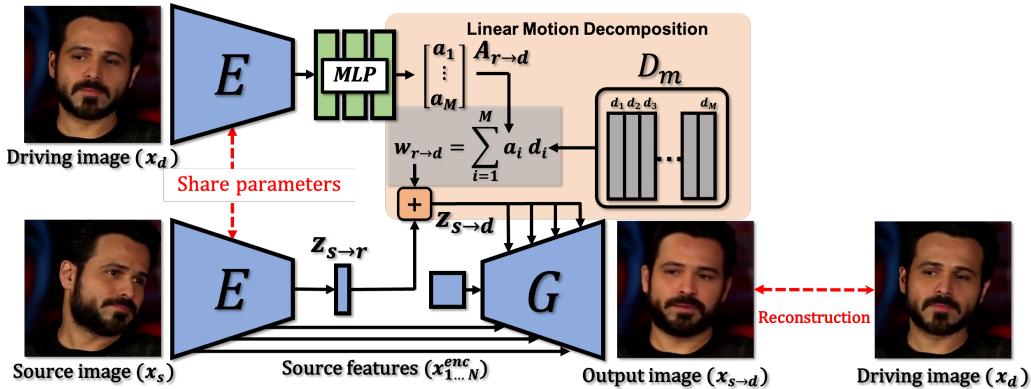


Figure 3: **Overview of LIA.** Our model is an auto-encoder consisting of two networks, an encoder E and a generator G . In the latent space, we apply Linear Motion Decomposition (LMD) towards learning a motion dictionary D_m , which is an orthogonal basis where each vector represents a basic visual transformation. LIA takes two frames sampled from the same video sequence as source image x_s and driving image x_d respectively during training. Firstly, it encodes x_s into a source latent code $z_{s \rightarrow r}$ and x_d into a magnitude vector $A_{r \rightarrow d}$. Then, it linearly combines $A_{r \rightarrow d}$ and a trainable D_m using LMD to obtain a latent path $w_{r \rightarrow d}$, which is used to navigate $z_{s \rightarrow r}$ to a target code $z_{s \rightarrow d}$. Finally, G decodes $z_{s \rightarrow d}$ into a target dense flow field and warps x_s to an output image $x_{s \rightarrow d}$. The training objective is to reconstruct x_d using $x_{s \rightarrow d}$.

3 METHOD

Self-supervised image animation aims at learning to transfer motion from a subject of a driving video to a subject in a source image based on training with a large video dataset. In this work, we propose to model such motion transformation via latent space navigation. The general pipeline is illustrated in Fig. 2. Specifically, for training, our model takes in a pair of source and driving images, randomly sampled from one video sequence. These two images are encoded into a latent code which is used to represent motion transformation in the image space. The training objective is to reconstruct the driving image by combining source image with learned motion transformation. For testing, frames of a driving video are sequentially processed with the source image to animate the source subject. We provide an overview of the proposed model in Fig. 3. Our model is an auto-encoder, consisting of two main networks, an encoder E and a generator G . In general, our model requires two steps to transfer motion. In the first step, E encodes source and driving images $x_s, x_d \sim \mathcal{X} \in \mathbb{R}^{3 \times H \times W}$ into latent codes in the latent space. The source code is then navigated into a target code, which is used to represent target motion transformation, along a learned latent path. Based on proposed Linear Motion Decomposition (LMD), we represent such a path as a linear combination of a set of learned motion directions and associated magnitudes, which are learned from x_d . In the second step, once the target latent code is obtained, G decodes it as a dense flow field $\phi_{s \rightarrow d} \sim \Phi \in \mathbb{R}^{2 \times H \times W}$ and uses $\phi_{s \rightarrow d}$ to warp x_s and then to obtain the output image. In the following, we proceed to discuss the two steps in detail.

3.1 LATENT MOTION REPRESENTATION

Given a source image x_s and a driving image x_d , our first step constitutes of learning a *latent code* $z_{s \rightarrow d} \sim \mathcal{Z} \in \mathbb{R}^N$ to represent the motion transformation from x_s to x_d . Due to the uncertainty of two images, directly learning $z_{s \rightarrow d}$ puts forward a high requirement on the model to capture a complex distribution of motion. Mathematically, it requires modeling directions and norms of the vector $z_{s \rightarrow d}$ simultaneously, which is challenging. Therefore, instead of modeling motion transformation $x_s \rightarrow x_d$, we assume there exists a reference image x_r and motion transfer can be modeled as $x_s \rightarrow x_r \rightarrow x_d$, where $z_{s \rightarrow d}$ is learned in an indirect manner. We model $z_{s \rightarrow d}$ as a target point in the latent space, which can be reached by taking linear walks from a starting point $z_{s \rightarrow r}$ along a linear path $w_{r \rightarrow d}$ (see Fig. 2), given by

$$z_{s \rightarrow d} = z_{s \rightarrow r} + w_{r \rightarrow d}, \quad (1)$$

where $z_{s \rightarrow r}$ and $w_{r \rightarrow d}$ indicate the transformation $x_s \rightarrow x_r$ and $x_r \rightarrow x_d$ respectively. Both $z_{s \rightarrow r}$ and $w_{r \rightarrow d}$ are learned independently and $z_{s \rightarrow r}$ is obtained by passing x_s through E .

We learn $w_{r \rightarrow d}$ via Linear Motion Decomposition (LMD). Our idea is to learn a set of motion directions $D_m = \{\mathbf{d}_1, \dots, \mathbf{d}_M\}$ to represent any path in the latent space. We constrain D_m as an orthogonal basis, where each vector indicates a motion direction \mathbf{d}_i . We then combine each vector in the basis with a vector $A_{r \rightarrow d} = \{a_1, \dots, a_M\}$, where a_i represents the magnitude of \mathbf{d}_i . Hence, any linear path in the latent space can be represented using a linear combination

$$w_{r \rightarrow d} = \sum_{i=1}^M a_i \mathbf{d}_i, \quad (2)$$

where $\mathbf{d}_i \in \mathbb{R}^N$ and $a_i \in \mathbb{R}$ for all $i \in \{1, \dots, M\}$. Semantically, each \mathbf{d}_i should represent a basic visual transformation and a_i indicates the required steps to walk in \mathbf{d}_i towards achieving $w_{r \rightarrow d}$. Due to D_m entailing an orthogonal basis, any two directions $\mathbf{d}_i, \mathbf{d}_j$ follow the constrain

$$\langle \mathbf{d}_i, \mathbf{d}_j \rangle = \begin{cases} 0 & i \neq j \\ 1 & i = j. \end{cases} \quad (3)$$

We implement D_m as a learnable matrix and apply the Gram-Schmidt process during each forward pass, in order to meet the requirement of orthogonality. $A_{r \rightarrow d}$ is obtained by mapping $z_{d \rightarrow r}$, which is the output of x_d after E , through a 5-layer MLP. The final formulation of latent motion representation for each x_s and x_d is thus given as

$$z_{s \rightarrow d} = z_{s \rightarrow r} + \sum_{i=1}^M a_i \mathbf{d}_i. \quad (4)$$

3.2 LATENT CODE DRIVEN IMAGE ANIMATION

Once we obtain $z_{s \rightarrow d}$, in our second step, we use G to decode a flow field $\phi_{s \rightarrow d}$ and warp x_s . Our G consists of two components, a flow field generator G_f and a refinement network G_r (we provide details in Appendix A).

Towards learning multi-scale features, G is designed as a residual network containing N models to produce a pyramid of flow fields $\phi_{s \rightarrow d} = \{\phi_i\}_1^N$ in different layers of G_f . Multi-scale source features $x_s^{enc} = \{x_i^{enc}\}_1^N$ are obtained from E and are warped in G_f .

However, as pointed out by Siarohin et al. (2019), only relying on $\phi_{s \rightarrow d}$ to warp source features is insufficient to precisely reconstruct driving images due to the existing occlusions in some positions of x_s . In order to predict pixels in those positions, the network is required to inpaint the warped feature maps. Therefore, we predict multi-scale masks $\{m_i\}_1^N$ along with $\{\phi_i\}_1^N$ in G_f to mask out the regions required to be inpainted. In each residual module, we have

$$x'_i = \mathcal{T}(\phi_i, x_i^{enc}) \odot m_i, \quad (5)$$

where \odot denotes the Hadamard product and \mathcal{T} denotes warping operation, whereas x'_i signifies the masked features. We generate both dense flow fields, as well as masks by letting each residual module output a 3-channel feature map in which the first two channels represent ϕ_i and the last channel m_i . Based on an inpainted feature map $f(x'_i)$, as well as an upsampled image $g(x_{i-1})$ provided by the previous module in G_r , the RGB image from each module is given by

$$o_i = f(x'_i) + g(o_{i-1}), \quad (6)$$

where f and g denote the inpainting and upsampling layers, respectively. The output image o_N from the last module constitutes the final generated image $x_{s \rightarrow d} = o_N$.

3.3 LEARNING

We train the LIA - framework in a self-supervised manner to reconstruct x_d using three losses, i.e., a reconstruction loss \mathcal{L}_{recon} , a perceptual loss \mathcal{L}_{vgg} (Johnson et al., 2016) and an adversarial loss \mathcal{L}_{adv} . We use \mathcal{L}_{recon} to minimize the pixel-wise L_1 distance between x_d and $x_{s \rightarrow d}$, calculated as

$$\mathcal{L}_{recon}(x_{s \rightarrow d}, x_d) = \mathbb{E}[\|x_d - x_{s \rightarrow d}\|_1]. \quad (7)$$

Towards minimizing the perceptual distance, we apply a VGG19-based \mathcal{L}_{vgg} on multi-scale feature maps between real and generated images, written as

$$\mathcal{L}_{vgg}(x_{s \rightarrow d}, x_d) = \mathbb{E}\left[\sum_n^N \|F_n(x_d) - F_n(x_{s \rightarrow d})\|_1\right], \quad (8)$$

where F_n denotes the n^{th} layer in a pre-trained VGG19 (Simonyan & Zisserman, 2015). In practice, towards penalizing real and generated images in multi-scale images, we use a pyramid of four resolutions, namely 256×256 , 128×128 , 64×64 and 32×32 as inputs of VGG19. The final perceptual loss is the addition of perceptual losses in four resolutions.

Further, towards generating photo-realistic results, we incorporate a non-saturating adversarial loss \mathcal{L}_{adv} on $x_{s \rightarrow d}$, which is calculated as

$$\mathcal{L}_{adv}(x_{s \rightarrow d}) = \mathbb{E}_{x_{s \rightarrow d} \sim p_{rec}}[-\log(D(x_{s \rightarrow d}))], \quad (9)$$

where D is a discriminator, aimed at distinguishing reconstructed from original images. Our full loss function is the combination of three losses with λ as a balanced hyperparameter

$$\mathcal{L}(x_{s \rightarrow d}, x_d) = \mathcal{L}_{recon}(x_{s \rightarrow d}, x_d) + \lambda \mathcal{L}_{vgg}(x_{s \rightarrow d}, x_d) + \mathcal{L}_{adv}(x_{s \rightarrow d}). \quad (10)$$

3.4 INFERENCE

In inference stage, given a driving video sequence $V_d = \{x_t\}_1^T$, we aim to transfer motion from V_d to x_s , in order to generate a novel video $V_{d \rightarrow s} = \{x_{t \rightarrow s}\}_1^T$. If V_d and x_s stem from the same video sequence, *i.e.*, $x_s = x_1$, our task comprises of reconstructing the entire original video sequence. Therefore, we construct the latent motion representation of each frame using *absolute transfer*, which follows the training process, given as

$$z_{s \rightarrow t} = z_{s \rightarrow r} + w_{r \rightarrow t}, \quad t \in \{1, \dots, T\}. \quad (11)$$

However, in real world applications, interest is rather placed on the scenario, where motion transfer between x_s and V_d , the latter stemming from different identities, *i.e.*, $x_s \neq x_1$. Taking a *talking head* video as an example, in this setting, beyond identity, x_1 and x_s might also differ in pose and expression. Therefore, we propose *relative transfer* to eliminate the motion impact of $w_{r \rightarrow 1}$ and involve motion of $w_{r \rightarrow s}$ in the full generated video sequence. Owing to a linear representation of the latent path, we can easily represent $z_{s \rightarrow t}$ for each frame as

$$\begin{aligned} z_{s \rightarrow t} &= (z_{s \rightarrow r} + w_{r \rightarrow s}) + (w_{r \rightarrow t} - w_{r \rightarrow 1}) \\ &= z_{s \rightarrow s} + (w_{r \rightarrow t} - w_{r \rightarrow 1}), \quad t \in \{1, \dots, T\}. \end{aligned} \quad (12)$$

In the first part of Eq. (12), $z_{s \rightarrow s}$ indicates the reconstruction of x_s , while the second part ($w_{r \rightarrow t} - w_{r \rightarrow 1}$) represents the motion from x_1 to x_t . This equation indicates that the original pose is preserved in x_s , at the same time motion is transferred from V_d . We note that in order to completely replicate the position and pose in V_d , relative motion transfer requires x_s and x_1 to contain similar poses, else face will have as starting image the pose from x_s rather than x_1 .

4 EXPERIMENTS

In this section, we firstly describe our experimental setup including implementation details and datasets. Secondly, we qualitatively demonstrate generated results based on testing datasets. Then, we provide quantitative evaluation *w.r.t.* image quality on (a) same-identity reconstruction, (b) cross-video motion transfer, presenting (c) a user study. Next, we conduct an ablation study that demonstrates (d) the effectiveness of our proposed motion dictionary, as well as (e) associated size. Finally, we provide an in-depth analysis of our (f) latent codes and (g) motion dictionary to interpret their semantic meanings.

Datasets Our model is trained on the datasets VoxCeleb (Chung et al., 2018), TaichiHD (Siarohin et al., 2019) and TED-talk (Siarohin et al., 2021). We follow the pre-processing method in (Siarohin et al., 2019) to crop frames into 256×256 resolution for quantitative evaluation. In addition, we process a 512×512 version of VoxCeleb towards qualitatively demonstrating the capacity of method on high resolution generation (see Appendix B.1).

Implementation details Our model is implemented in PyTorch (Paszke et al., 2019). All models are trained on four 16G NVIDIA V100 GPUs. The total batch size is 32 with 8 images per GPU. We use a learning rate of 0.002 to train our model with the Adam optimizer (Kingma & Ba, 2014). The dimension of all latent codes, as well as directions in D_m are set to be 512. In our loss function, we use $\lambda = 10$ in order to penalize more on the perceptual loss. It takes around 150 hours to fully train our framework.

Evaluation metrics We evaluate our model *w.r.t.* (i) reconstruction faithfulness using \mathcal{L}_1 , LPIPS, (ii) generated video quality using video FID, as well as (iii) semantic consistency using average keypoint distance (AKD), missing keypoint rate (MKR) and average euclidean distance (AED). Details are available in Appendix B.2.



Figure 4: **Qualitative results.** Examples for same-dataset *absolute motion transfer* on TaichiHD (top-right) and TED-talk (bottom-right). On VoxCeleb (left), we demonstrate cross-dataset *relative motion transfer*. We successfully transfer motion between x_1 and x_t from videos in VoxCeleb to x_s from FFHQ, the latter not being used for training.

4.1 QUALITATIVE RESULTS

Firstly, we evaluate the ability of LIA to generate realistic videos and compare related results with four state-of-the-art methods. For TaichiHD and TED-talk datasets, we conduct an experiment related to cross-video generation. Corresponding results (see Fig. 4) confirm that our method is able to correctly transfer motion on articulated human bodies, in the absence of explicit structure representations. For the VoxCeleb dataset, we conduct a cross-dataset generation-experiment, where we transfer motion from VoxCeleb to images of the FFHQ dataset (Karras et al., 2019). We observe that our method outperforms FOMM and MRAA *w.r.t.* image quality, as both approaches deform the shape of original faces visibly. This is specifically notable in the case that source and driving images entail large pose variations. At the same time, LIA is able to successfully tackle this challenge and no similar deformations are visible.

4.2 COMPARISON WITH STATE-OF-THE-ART METHODS

We quantitatively compare our method with the state-of-the-art approaches X2Face, Monkey-Net, FOMM and MRAA on two tasks, namely (a) same-identity reconstruction and (b) cross-video motion transfer. Additionally, we conduct a (c) user study.

(a) Same-identity reconstruction We here evaluate the reconstruction ability of our method. Specifically, we reconstruct each testing video by using the first frame as x_s and the remaining frames as x_d . Results on three datasets are reported in Table 1. Focusing on foreground-reconstruction, our method outperforms the other approaches *w.r.t.* all metrics. More results are presented in Appendix B.3, discussing background-reconstruction.

Table 1: **Same-identity reconstruction.** Comparison with state-of-the-art methods on three datasets.

Method	VoxCeleb				TaichiHD				TED-talks			
	\mathcal{L}_1	AKD	AED	LPIPS	\mathcal{L}_1	(AKD, MKR)	AED	LPIPS	\mathcal{L}_1	(AKD, MKR)	AED	LPIPS
X2Face	0.078	7.687	0.405	-	0.080	(17.654, 0.109)	-	-	-	-	-	-
Monkey-Net	0.049	1.878	0.199	-	0.077	(10.798, 0.059)	-	-	-	-	-	-
FOMM	0.046	1.395	0.141	0.136	0.063	(6.472, 0.032)	0.495	0.191	0.030	(3.759, 0.0090)	0.428	0.13
MRAA <i>w/o</i> bg	0.043	1.307	0.140	0.127	0.063	(5.626, 0.025)	0.460	0.189	0.029	(3.126, 0.0092)	0.396	0.12
Ours	0.041	1.353	0.138	0.123	0.057	(4.823, 0.020)	0.431	0.180	0.027	(3.141, 0.0095)	0.399	0.11

(b) Cross-video motion transfer Next, we conduct experiments, where source images and driving videos stem from different video sequences. In this context, we mainly focus on evaluating *talking*

Table 2: **Cross-video generation.** We report video FID for both inner-dataset and cross-dataset tasks on VoxCeleb and GermanAudio datasets.

	VoxCeleb	GermanAudio
FOMM	0.323	0.456
MRAA	0.308	0.454
Ours	0.161	0.406

Table 4: **Ablation study on effectiveness of motion dictionary.** We conduct experiments on three datasets with and without D_m and show reconstruction results.

Method	VoxCeleb		TaichiHD		TED-talks	
	\mathcal{L}_1	LPIPS	\mathcal{L}_1	LPIPS	\mathcal{L}_1	LPIPS
w/o D_m	0.049	0.165	0.062	0.186	0.031	0.12
Full	0.041	0.123	0.057	0.180	0.028	0.11

Table 3: **User study**

	VoxCeleb(%)	TaichiHD(%)	TED-talk(%)
Ours/FOMM	92.9/7.1	64.5/35.5	71.4/28.6
Ours/MRAA	89.7/10.3	60.7/39.9	54.8/45.2

Table 5: **Ablation study on D_m size.**

M	VoxCeleb		TaichiHD		TED-talks	
	\mathcal{L}_1	LPIPS	\mathcal{L}_1	LPIPS	\mathcal{L}_1	LPIPS
5	0.051	0.15	0.070	0.22	0.037	0.15
10	0.043	0.13	0.065	0.20	0.036	0.13
20	0.041	0.12	0.057	0.18	0.028	0.11
40	0.042	0.12	0.060	0.19	0.030	0.12
100	0.041	0.12	0.058	0.18	0.028	0.11

head videos and explore two different cases. In the first case, we generate videos using the VoxCeleb testing set to conduct *motion transfer*. In the second case, source images are from an unseen dataset, namely the GermanAudio dataset (Thies et al., 2020), as we conduct *cross-dataset motion transfer*. In both experiments, we randomly construct source and driving pairs and transfer motion from driving videos to source images to generate a novel manipulated dataset. Since ground truth data for our generated videos is not available, we use video FID (as initialized by Wang et al. (2020b)) to compute the distance between generated and real data distributions. As shown in Tab. 2, our method outperforms all other approaches *w.r.t.* video FID, indicating the best generated video quality.

(c) **User study** We conduct a user study to evaluate subjective video quality. Towards this, we displayed paired videos and asked 20 human raters ‘which clip is more realistic’. Each video-pair contains a generated video from our method, as well as a video generated from FOMM or MRAA. Results suggest that our results are more realistic in comparison to FOMM and MRAA across all three datasets (see Tab. 3). Hence, the obtained human preference is in accordance with our quantitative evaluation.

4.3 ABLATION STUDY

We here analyze our proposed motion dictionary and focus on answering following two questions.

(d) **Is the motion dictionary D_m beneficial?** We here explore the impact of proposed D_m , by training our model without D_m . Specifically, we output $w_{r \rightarrow d}$ directly from MLPs, without using LMD to learn an orthogonal basis. From the evaluation results reported in Tab. 4, we observe that in the absence of D_m , LIA fails to generate high-quality images, which proves the effectiveness of D_m , consistently on all datasets. We show qualitative results in Appendix B.7.

(e) **How many directions are required in D_m ?** Towards finding an effective size of D_m , we empirically test three different M , viz. 5, 10, 20, 40 and 100. Quantitative results in Tab. 5 show that when using 20 directions, we obtain the best reconstruction results.

4.4 FURTHER ANALYSIS

(f) **Latent code analysis.** While our method successfully transfers motion via latent space navigation, we here aim at answering the question — *what does x_r represent?* Towards answering this question, we proceed to visualize x_r . We firstly decode $z_{s \rightarrow r}$ into a dense flow field $\phi_{s \rightarrow r}$, which then warps x_s . Fig. 5 shows examples of x_s and x_r . Interestingly, we observe that x_r represents the *canonical pose* of x_s , regardless of original poses of the subjects. And for all datasets, reference images resemble each other *w.r.t.* pose and scale. As such reference images can be considered as a normalized form of x_s , learning transformations between x_s and x_d using $x_s \rightarrow x_r \rightarrow x_d$ is considerably more efficient than $x_s \rightarrow x_d$, once x_r is fixed.

Noteworthy, we found a similar idea of learning a ‘reference image’ explored by Siarohin et al. (2019) (FOMM) and by Wiles et al. (2018) (X2Face). However, deviating from our visualized ‘reference image’, in FOMM it refers to a non-visualized and abstract concept. In contrast to X2Face,



Figure 5: **Visualization of reference images.** Example source (top) and reference images (down) from VoxCeleb, TaichiHD and TED-talk datasets. Our network learns *reference images* of a consistently frontal pose, systematically for all input images of each dataset.



Figure 6: **Linear manipulation of four motion directions on the painting of Mona Lisa.** Manipulated results indicate that d_6 represents *eye movement*, d_8 represents *head nodding*, whereas d_{19} and d_7 represent facial expressions.

we only require a latent code $z_{s \rightarrow r}$, rather than its explicit form $\phi_{s \rightarrow r}$ and x_r during both, training and testing.

(g) Motion dictionary interpretation. Towards further interpretation of directions in D_m , we conduct linear manipulations on each d_i . Details of the analysis are provided in Appendix B.5. Images pertained to manipulating four motion directions are depicted in Fig. 6. The results suggest that the directions in D_m are semantically meaningful, as they represent basic visual transformations such as head nodding (d_8), eye movement (d_6) and facial expressions (d_{19} and d_7).

5 CONCLUSIONS

In this paper, we presented a novel self-supervised auto-encoder LIA, aimed at animating images via latent space navigation. By the proposed Linear Motion Decomposition (LMD), we were able to formulate the task of transferring motion from driving videos to source images as learning linear transformations in the latent space. We evaluated proposed method on real-world videos and demonstrated that our approach is able to successfully animate still images, while eliminating the necessity of *explicit structure representations*. In addition, we showed that the incorporated motion dictionary is interpretable and contains directions pertaining to basic visual transformations. Both quantitative and qualitative evaluations showed that LIA outperforms state-of-art algorithms on all benchmarks. We postulate that LIA opens a new door in design of interpretable generative models for video generation.

Public release. We intend to release our source code, as well as trained models. Moreover, we will release a dataset of videos, generated by LIA, in order to facilitate research on deepfake detection.

REFERENCES

- Rameen Abdal, Yipeng Qin, and Peter Wonka. Image2stylegan++: How to edit the embedded images? In *Proceedings of the IEEE/CVF Conference on Computer Vision and Pattern Recognition (CVPR)*, June 2020.
- Brandon Amos, Bartosz Ludwiczuk, and Mahadev Satyanarayanan. Openface: A general-purpose face recognition library with mobile applications. Technical report, CMU-CS-16-118, CMU School of Computer Science, 2016.
- Andrew Brock, Jeff Donahue, and Karen Simonyan. Large scale GAN training for high fidelity natural image synthesis. In *ICLR*, 2019.
- Adrian Bulat and Georgios Tzimiropoulos. How far are we from solving the 2d & 3d face alignment problem? (and a dataset of 230,000 3d facial landmarks). In *ICCV*, 2017.
- Chen Cao, Qiming Hou, and Kun Zhou. Displaced dynamic expression regression for real-time facial tracking and animation. *ACM Transactions on graphics (TOG)*, 33(4):1–10, 2014.
- Z. Cao, G. Hidalgo Martinez, T. Simon, S. Wei, and Y. A. Sheikh. Openpose: Realtime multi-person 2d pose estimation using part affinity fields. *IEEE Transactions on Pattern Analysis and Machine Intelligence*, 2019.
- Caroline Chan, Shiry Ginosar, Tinghui Zhou, and Alexei A Efros. Everybody dance now. In *ICCV*, 2019.
- J. S. Chung, A. Nagrani, and A. Zisserman. Voxceleb2: Deep speaker recognition. In *INTER-SPEECH*, 2018.
- Aidan Clark, Jeff Donahue, and Karen Simonyan. Adversarial video generation on complex datasets. *arXiv preprint arXiv:1907.06571*, 2019.
- Lore Goetschalckx, Alex Andonian, Aude Oliva, and Phillip Isola. Ganalyze: Toward visual definitions of cognitive image properties. In *ICCV*, pp. 5744–5753, 2019.
- Kensho Hara, Hirokatsu Kataoka, and Yutaka Satoh. Can spatiotemporal 3d cnns retrace the history of 2d cnns and imagenet? In *CVPR*, 2018.
- Martin Heusel, Hubert Ramsauer, Thomas Unterthiner, Bernhard Nessler, and Sepp Hochreiter. Gans trained by a two time-scale update rule converge to a local nash equilibrium. In *NIPS*, 2017.
- Phillip Isola, Jun-Yan Zhu, Tinghui Zhou, and Alexei A Efros. Image-to-Image Translation with Conditional Adversarial Networks. In *CVPR*, 2017.
- Ali Jahanian, Lucy Chai, and Phillip Isola. On the "steerability" of generative adversarial networks. In *ICLR*, 2020.
- Yunseok Jang, Gunhee Kim, and Yale Song. Video Prediction with Appearance and Motion Conditions. In *ICML*, 2018.
- Justin Johnson, Alexandre Alahi, and Li Fei-Fei. Perceptual losses for real-time style transfer and super-resolution. In *European conference on computer vision*, pp. 694–711. Springer, 2016.
- Tero Karras, Samuli Laine, and Timo Aila. A style-based generator architecture for generative adversarial networks. In *CVPR*, 2019.
- Tero Karras, Samuli Laine, Miika Aittala, Janne Hellsten, Jaakko Lehtinen, and Timo Aila. Analyzing and improving the image quality of StyleGAN. In *CVPR*, 2020.
- Diederik P Kingma and Jimmy Ba. Adam: A method for stochastic optimization. *arXiv preprint arXiv:1412.6980*, 2014.
- Alex Krizhevsky, Ilya Sutskever, and Geoffrey E Hinton. Imagenet classification with deep convolutional neural networks. In F. Pereira, C. J. C. Burges, L. Bottou, and K. Q. Weinberger (eds.), *Advances in Neural Information Processing Systems*, 2012.

- Yijun Li, Chen Fang, Jimei Yang, Zhaowen Wang, Xin Lu, and Ming-Hsuan Yang. Flow-grounded spatial-temporal video prediction from still images. In *ECCV*, 2018.
- Arsha Nagrani, Joon Son Chung, Weidi Xie, and Andrew Zisserman. Voxceleb: Large-scale speaker verification in the wild. *Computer Science and Language*, 2019.
- Katsunori Ohnishi, Shohei Yamamoto, Yoshitaka Ushiku, and Tatsuya Harada. Hierarchical video generation from orthogonal information: Optical flow and texture. In *AAAI*, 2018.
- Junting Pan, Chengyu Wang, Xu Jia, Jing Shao, Lu Sheng, Junjie Yan, and Xiaogang Wang. Video generation from single semantic label map. *arXiv preprint arXiv:1903.04480*, 2019.
- Adam Paszke, Sam Gross, Francisco Massa, Adam Lerer, James Bradbury, Gregory Chanan, Trevor Killeen, Zeming Lin, Natalia Gimelshein, Luca Antiga, Alban Desmaison, Andreas Kopf, Edward Yang, Zachary DeVito, Martin Raison, Alykhan Tejani, Sasank Chilamkurthy, Benoit Steiner, Lu Fang, Junjie Bai, and Soumith Chintala. Pytorch: An imperative style, high-performance deep learning library. In H. Wallach, H. Larochelle, A. Beygelzimer, F. d'Alché-Buc, E. Fox, and R. Garnett (eds.), *Advances in Neural Information Processing Systems*. 2019.
- William Peebles, John Peebles, Jun-Yan Zhu, Alexei A. Efros, and Antonio Torralba. The hessian penalty: A weak prior for unsupervised disentanglement. In *Proceedings of European Conference on Computer Vision (ECCV)*, 2020.
- JK Rowling. Harry potter. *The 100 Greatest Literary Characters*, pp. 183, 2019.
- Joanne Kathleen Rowling, John Tiffany, and Jack Thorne. *Harry Potter and the Cursed Child—Parts One and Two (Special Rehearsal Edition)*. Pottermore Publishing, 2016.
- Masaki Saito, Eiichi Matsumoto, and Shunta Saito. Temporal generative adversarial nets with singular value clipping. In *ICCV*, 2017.
- Yujun Shen and Bolei Zhou. Closed-form factorization of latent semantics in gans. In *CVPR*, 2021.
- Yujun Shen, Jinjin Gu, Xiaoou Tang, and Bolei Zhou. Interpreting the latent space of gans for semantic face editing. In *CVPR*, 2020.
- Aliaksandr Siarohin, Stéphane Lathuilière, Sergey Tulyakov, Elisa Ricci, and Nicu Sebe. First order motion model for image animation. In H. Wallach, H. Larochelle, A. Beygelzimer, F. d'Alché-Buc, E. Fox, and R. Garnett (eds.), *Advances in Neural Information Processing Systems*, volume 32. Curran Associates, Inc., 2019. URL <https://proceedings.neurips.cc/paper/2019/file/31c0b36aef265d9221af80872ceb62f9-Paper.pdf>.
- Aliaksandr Siarohin, Oliver Woodford, Jian Ren, Menglei Chai, and Sergey Tulyakov. Motion representations for articulated animation. In *CVPR*, 2021.
- Karen Simonyan and Andrew Zisserman. Very deep convolutional networks for large-scale image recognition. In *International Conference on Learning Representations*, 2015.
- Justus Thies, Michael Zollhofer, Marc Stamminger, Christian Theobalt, and Matthias Nießner. Face2face: Real-time face capture and reenactment of RGB videos. In *CVPR*, pp. 2387–2395, 2016.
- Justus Thies, Michael Zollhöfer, and Matthias Nießner. Deferred neural rendering: Image synthesis using neural textures. *ACM Transactions on Graphics (TOG)*, 38(4):1–12, 2019.
- Justus Thies, Mohamed Elgharib, Ayush Tewari, Christian Theobalt, and Matthias Nießner. Neural voice puppetry: Audio-driven facial reenactment. *ECCV*, 2020.
- Yu Tian, Jian Ren, Menglei Chai, Kyle Olszewski, Xi Peng, Dimitris N. Metaxas, and Sergey Tulyakov. A good image generator is what you need for high-resolution video synthesis. In *International Conference on Learning Representations*, 2021. URL <https://openreview.net/forum?id=6puCSjH3hWA>.
- Sergey Tulyakov, Ming-Yu Liu, Xiaodong Yang, and Jan Kautz. MoCoGAN: Decomposing motion and content for video generation. In *CVPR*, 2018.

- Carl Vondrick, Hamed Pirsiavash, and Antonio Torralba. Generating videos with scene dynamics. In *NIPS*, 2016.
- Andrey Voynov and Artem Babenko. Unsupervised discovery of interpretable directions in the gan latent space. *arXiv preprint arXiv:2002.03754*, 2020.
- Jacob Walker, Kenneth Marino, Abhinav Gupta, and Martial Hebert. The pose knows: Video forecasting by generating pose futures. In *ICCV*, 2017.
- Ting-Chun Wang, Ming-Yu Liu, Jun-Yan Zhu, Guilin Liu, Andrew Tao, Jan Kautz, and Bryan Catanzaro. Video-to-video synthesis. In *NeurIPS*, 2018.
- Ting-Chun Wang, Ming-Yu Liu, Andrew Tao, Guilin Liu, Jan Kautz, and Bryan Catanzaro. Few-shot video-to-video synthesis. In *NeurIPS*, 2019.
- Ting-Chun Wang, Arun Mallya, and Ming-Yu Liu. One-shot free-view neural talking-head synthesis for video conferencing. In *Proceedings of the IEEE Conference on Computer Vision and Pattern Recognition*, 2021a.
- Yaohui Wang, Piotr Bilinski, Francois Bremond, and Antitza Dantcheva. Imaginator: Conditional spatio-temporal gan for video generation. In *The IEEE Winter Conference on Applications of Computer Vision (WACV)*, March 2020a.
- Yaohui Wang, Piotr Bilinski, Francois Bremond, and Antitza Dantcheva. G3AN: Disentangling appearance and motion for video generation. In *CVPR*, 2020b.
- Yaohui Wang, Francois Bremond, and Antitza Dantcheva. Inmodegan: Interpretable motion decomposition generative adversarial network for video generation. *arXiv preprint arXiv:2101.03049*, 2021b.
- Olivia Wiles, A Koepke, and Andrew Zisserman. X2face: A network for controlling face generation using images, audio, and pose codes. In *Proceedings of the European conference on computer vision (ECCV)*, pp. 670–686, 2018.
- Ceyuan Yang, Zhe Wang, Xinge Zhu, Chen Huang, Jianping Shi, and Dahua Lin. Pose guided human video generation. In *ECCV*, 2018.
- Egor Zakharov, Aliaksandra Shysheya, Egor Burkov, and Victor Lempitsky. Few-shot adversarial learning of realistic neural talking head models. In *ICCV*, 2019.
- Richard Zhang, Phillip Isola, Alexei A Efros, Eli Shechtman, and Oliver Wang. The unreasonable effectiveness of deep features as a perceptual metric. In *CVPR*, 2018.
- Long Zhao, Xi Peng, Yu Tian, Mubbasir Kapadia, and Dimitris Metaxas. Learning to forecast and refine residual motion for image-to-video generation. In *ECCV*, 2018.
- Zhedong Zheng, Tao Ruan, Yunchao Wei, Yi Yang, and Tao Mei. Vehiclenet: Learning robust visual representation for vehicle re-identification. *IEEE Transaction on Multimedia (TMM)*, 2020.
- Jiapeng Zhu, Yujun Shen, Deli Zhao, and Bolei Zhou. In-domain gan inversion for real image editing. In *Proceedings of European Conference on Computer Vision (ECCV)*, 2020.

A DETAILS OF MODEL ARCHITECTURE

We proceed to describe the model architecture in this section. Fig. 7 shows details of our E . In each ResBlock in E , spatial size of input feature maps are downsampled. We take feature maps of spatial sizes from 8×8 to 256×256 as our appearance features x_i^{enc} . We use a 5-layer MLP to predict a magnitude vector $A_{d \rightarrow r}$ from $z_{d \rightarrow r}$. Fig. 8 (a) shows the general architecture of our G , which consists of two components, a flow field generator G_f and a refinement network G_r . We apply *StyleConv* (Upsample + Conv3 \times 3), which is proposed by StyleGAN2, in G_f . *StyleConv* takes latent representation $z_{s \rightarrow t}$ as style code and generates flow field ϕ_i and corresponding mask m_i . G_r uses *UpConv* (Conv1 \times 1 + Upsample) to upsample and refine inpainted feature maps to target resolution. We show details pertaining to G block in Fig. 8 (b). Each G block is used to upsample $\times 2$ the previous resolution. We stack 6 blocks towards producing 256 resolution images.

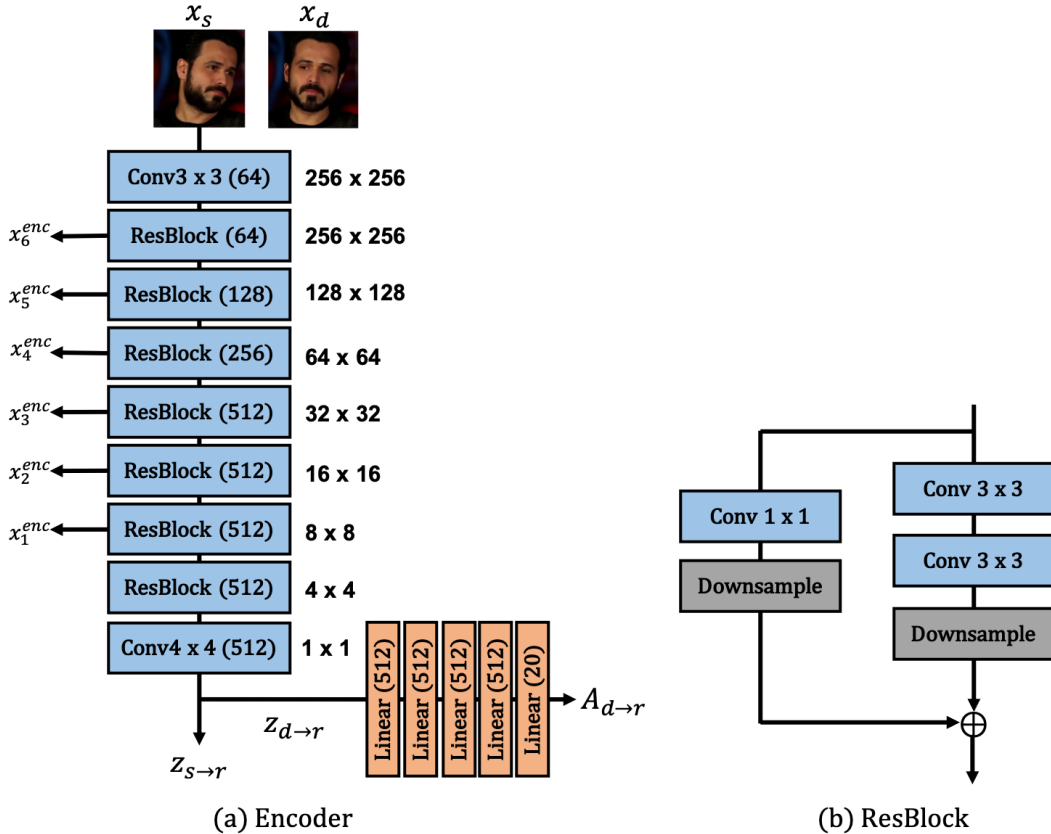


Figure 7: **Encoder architecture.** We show details about architecture of E in (a) and ResBlock in (b).

B EXPERIMENTS

We proceed to introduce details of datasets and evaluation metrics used in our experiments.

B.1 DATASETS

VoxCeleb (Nagrani et al., 2019) consists of a large amount of interview videos of different celebrities. Following the process of FOMM (Siarohin et al., 2019), we extract frames and crop them into 256×256 resolution. In total, VoxCeleb contains a training set of 17928 videos and a test set of 495 videos.

TaiChiHD (Siarohin et al., 2019) consists of videos of full human bodies performing Tai Chi actions. We follow the original pre-processing of FOMM (Siarohin et al., 2019) and utilize its 256×256 version. TaiChiHD contains 1096 training videos and 115 testing videos.

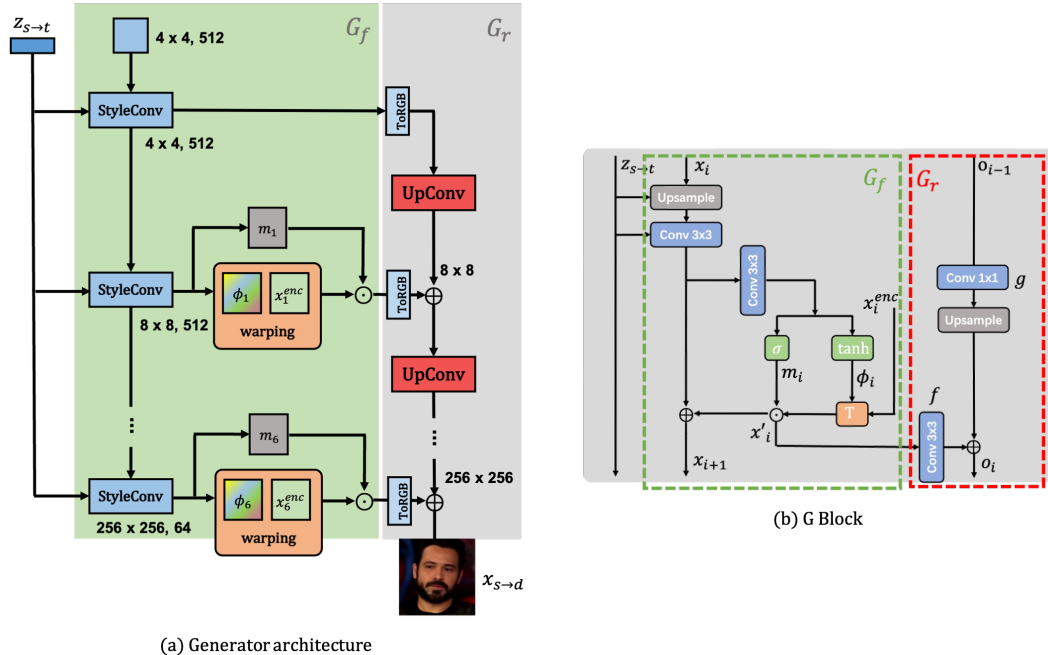


Figure 8: **Generator architecture.** We show details about architecture of G in (a) and G block in (b).

TED-talk is a new dataset proposed in MRAA (Siarohin et al., 2021). It comprises a number of TED-talk videos, where the main subjects have been cropped out. We resize the original version into 256×256 resolution to train our model. This dataset includes 1124 training videos and 130 testing videos.

B.2 EVALUATION METRICS

We use five different metrics to evaluate our experimental results, namely \mathcal{L}_1 , LPIPS, AKD, MKR and AED that quantify the reconstructed results. In addition, we compute video FID to evaluate video quality in motion transferring tasks.

\mathcal{L}_1 represents the mean absolute pixel difference between reconstructed and real videos.

LPIPS (Zhang et al., 2018) aims at measuring the perceptual similarity between reconstructed and real images by leveraging the deep features from AlexNet (Krizhevsky et al., 2012).

Video FID is a modified version of original FID (Heusel et al., 2017). We here follow the same implementation as Wang et al. (2020b) and utilize a pre-trained ResNext101 (Hara et al., 2018) to extract spatio-temporal features to compute the distance between real and generated videos distributions. We take the first 100 frames of each video as input of the feature-extractor to compute the final scores.

Average keypoint distance (AKD) and missing keypoint rate (MKR) evaluate the difference between keypoints of reconstructed and ground truth videos. We extract landmarks using the face alignment approach of (Bulat & Tzimiropoulos, 2017) and extract body poses for both TaiChiHD and TED-talks using OpenPose (Cao et al., 2019). AKD is computed as the average distance between corresponding keypoints, whereas MKR is the proportion of keypoints present in the ground-truth that are missing in a reconstructed video.

Average Euclidean distance (AED) measures the ability of preserving identity in reconstructed video. We use a person re-identification pretrained model (Zheng et al., 2020) for measuring human bodies (TaiChiHD and TED-talk) and OpenFace (Amos et al., 2016) for faces to extract identity embeddings from reconstructed and ground truth frame pairs, then we compute MSE of their difference for all pairs.

B.3 COMPARISON WITH FULL MRAA

We show quantitative evaluation results with the full MRAA model in Tab. 6. We observe that our method achieves competitive results in reconstruction and keypoint evaluation. *W.r.t.* the TaiChiHD

dataset, while we do not explicitly predict keypoints, interestingly we outperform MRAA in both, AKD and MKR. Such results showcase the effectiveness of our proposed method on modeling articulated human structures. However, reconstruction evaluation cannot provide a completely fair comparison on how well the main subjects (*e.g.*, faces and human bodies) are generated in videos. This is in particular the case for TaichiHD and TED-talk, where backgrounds have large contributions to the final scores.

Table 6: Comparison with full MRAA.

Method	VoxCeleb				TaichiHD				TED-talks			
	\mathcal{L}_1	AKD	AED	LPIPS	\mathcal{L}_1	(AKD, MKR)	AED	LPIPS	\mathcal{L}_1	(AKD, MKR)	AED	LPIPS
MRAA	0.041	1.303	0.135	0.124	0.045	(5.551, 0.025)	0.431	0.178	0.027	(3.107, 0.0093)	0.379	0.11
Ours	0.041	1.353	0.138	0.123	0.057	(4.823, 0.020)	0.431	0.180	0.027	(3.141, 0.0095)	0.399	0.11

B.4 REFERENCE IMAGE GENERATION.

To produce x_r , we use G to decode $z_{s \rightarrow r}$ into the flow field $\phi_{s \rightarrow r}$. Reference image x_r is obtained by warping x_s using $\phi_{s \rightarrow r}$. The entire process is shown in Fig. 9.

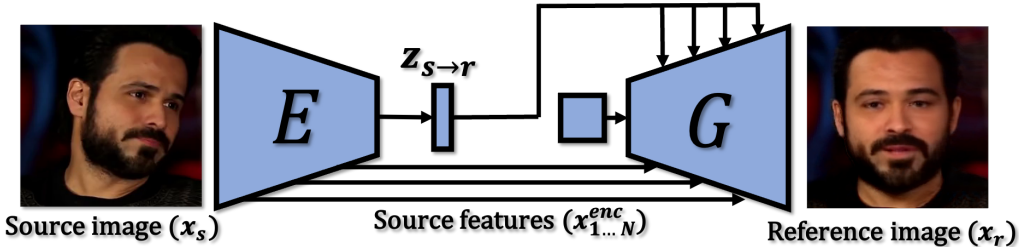


Figure 9: Reference image generation.

B.5 MANIPULATION IN MOTION DICTIONARY

Towards interpreting D_m , we firstly obtain $z_{s \rightarrow r}$ and $A_{r \rightarrow s}$ from the encoder by reconstructing x_s . From Eq. (4), we obtain

$$z_{s \rightarrow s} = z_{s \rightarrow r} + w_{r \rightarrow s}, \tag{13}$$

$$w_{r \rightarrow s} = \sum_{i=1}^M a_i \mathbf{d}_i. \tag{14}$$

Our interpretation is based on linearly manipulating each \mathbf{d}_i in D_m . We compute a_{min} and a_{max} for each \mathbf{d}_i for reconstructing the training data and use them as a manipulation range $[a_{min}, a_{max}]$. The manipulation step size is computed as

$$\frac{a_{max} - a_{min}}{n}, \tag{15}$$

where n indicates the total steps. The manipulated magnitude is then given by

$$a' = \frac{s(a_{max} - a_{min})}{n}, s \in [1...n]. \tag{16}$$

We use a' to replace a_i . Hence the latent code for the the manipulated image is given by

$$z_{s \rightarrow m} = z_{s \rightarrow r} + w_{r \rightarrow m}, \tag{17}$$

$$w_{r \rightarrow m} = a'_i \mathbf{d}_i, i \in [1...M]. \tag{18}$$

When manipulating each \mathbf{d}_i , we eliminate the contributions of other directions by setting

$$a'_j = 0, \text{ if } j \neq i. \tag{19}$$

We show more manipulation results in Fig. 10.

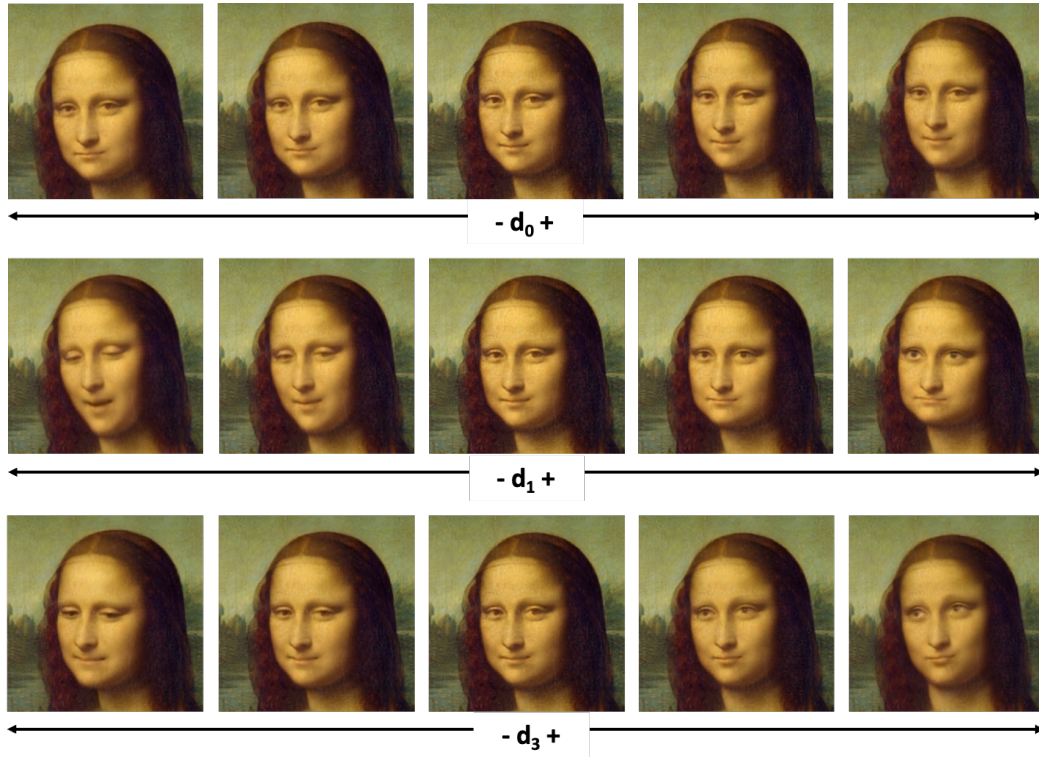


Figure 10: Manipulation of motion dictionary.

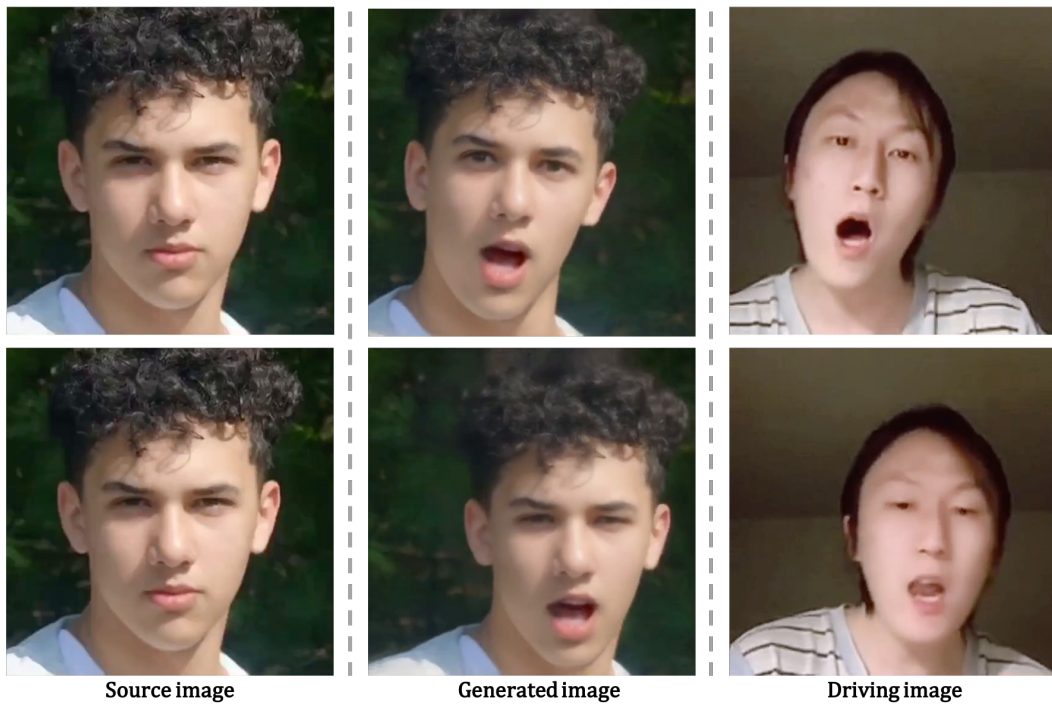


Figure 11: High resolution generation Image animation using a real-world driving video.



Figure 12: **Generated results with and without motion dictionary.**

B.6 QUALITATIVE RESULTS ON HIGH RESOLUTION GENERATION

We show generated results on 512×512 resolution for *talking head* images. We train LIA using VoxCeleb, with resolution 512×512 and show motion transfer results using a real-world driving video in Fig. 11.

B.7 QUALITATIVE RESULTS ON EFFECTIVENESS OF USING MOTION DICTIONARY

Fig. 12 illustrates the generated results on transferring motion from VoxCeleb to GermanAudio with and without motion dictionary. We observe that without the motion dictionary, appearance information is undesirably transferred from driving videos to generated videos.

B.8 ORTHOGONALITY ANALYSIS IN MOTION DICTIONARY.

We provided comparison in Tab. 7 to analyze the effectiveness of orthogonality in the motion dictionary. In non-orthogonality experiments, we randomly initialize 20 directions without using Gram-Schmidt process. Tab. 7 shows that models using orthogonal basis perform better than the ones using non-orthogonal basis. To further analyze the correlation between each direction after training, we also computed angles between direction pairs in the motion dictionary for three datasets and show results in Fig. 13, Fig. 14 and Fig. 16. We observe that most of the directions are nearly orthogonal after training and angles are $90^\circ \pm 10^\circ$. Therefore we consider on current three training datasets that employing an orthogonal basis is effective. However, there are other factors that may affect such choice, e.g., complexity of the datasets and latent code dimension. It remains an open question whether orthogonality is a general solution for all cases or just in our context.

B.9 LIMITATIONS

For human body, one limitation of our method is dealing with body occlusion. We observe in Fig. 16 that in taichi videos, in case of occlusion cause by legs and arms, motion is not transferred successfully. In addition, in TED-talks, transferring hand motion is challenging, as hands are of small size, articulated and sometimes occluded by human bodies.

Table 7: Comparison between models using orthogonal and non-orthogonal bases

	VoxCeleb		TaichiHD		TED-talks	
	\mathcal{L}_1	LPIPS	\mathcal{L}_1	LPIPS	\mathcal{L}_1	LPIPS
None-orthogonal	0.044	0.13	0.060	0.18	0.030	0.12
Orthogonal	0.041	0.12	0.057	0.18	0.028	0.11

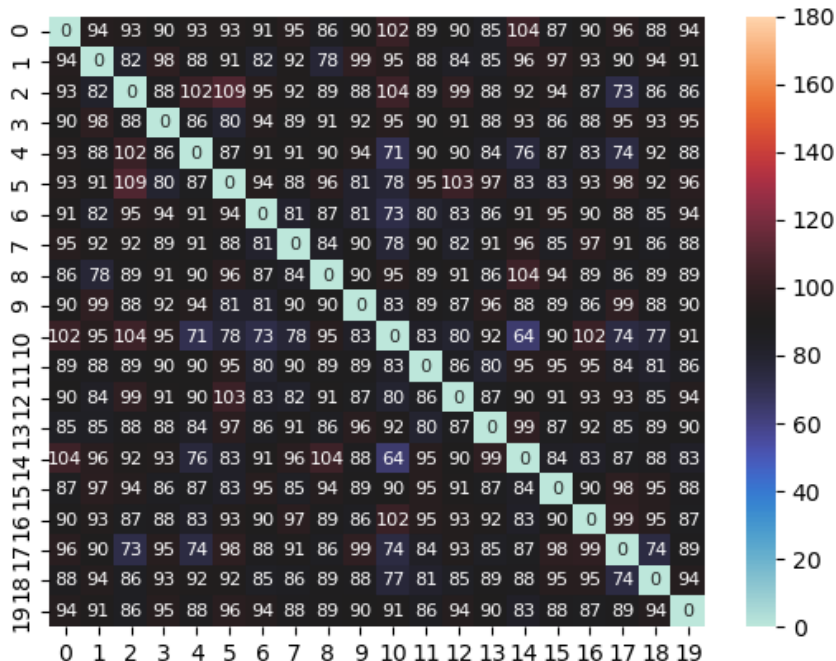


Figure 13: Analysis on non-orthogonal basis. Cross-direction angle (degree) analysis on VoxCeleb.

C ETHIC STATEMENT

In this work, we aim to synthesize high-quality videos by transferring motion on still images. Our approach can be used for movie production, making video games, online education, generating synthetic data for other computer vision tasks, etc. We note that our framework mainly focuses on learning how to model motion distribution rather than directly model appearance, therefore it is not biased towards any specific gender, race, region, or social class. It works equally well irrespective of the difference in subjects.

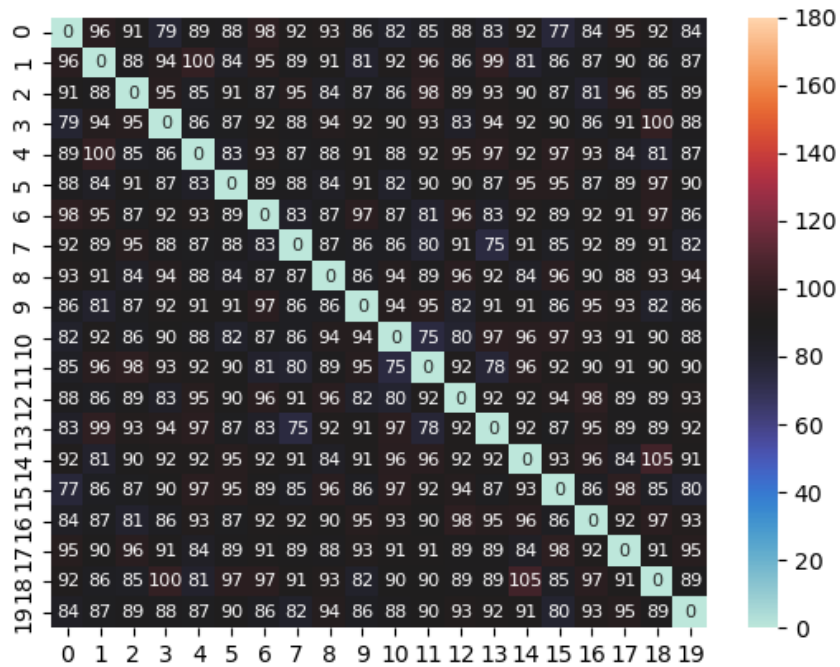


Figure 14: **Analysis on non-orthogonal basis.** Cross-direction angle (degree) analysis on TaichiHD.

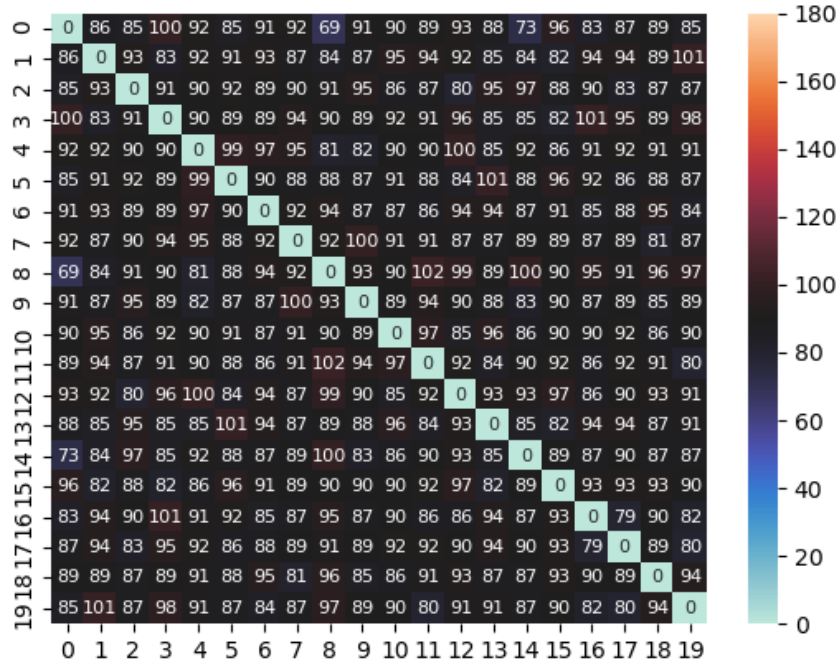


Figure 15: **Analysis on non-orthogonal basis.** Cross-direction angle (degree) analysis on TED-talks.

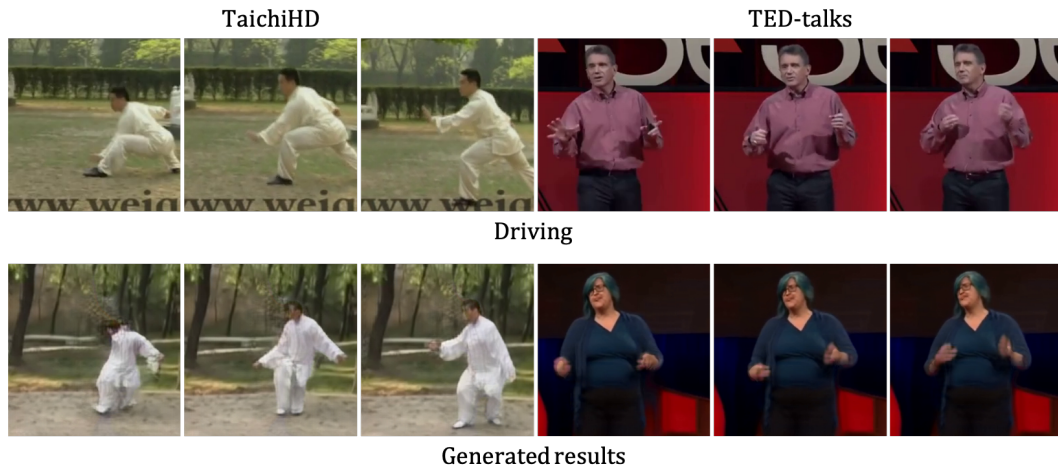


Figure 16: Failure cases.